Zebrafish as research model to study Gaucher disease: Insights into molecular mechanisms

Lelieveld, L.T.

CHAPTER 2

Biochemical evaluation and comparison of GCase enzymes of different species

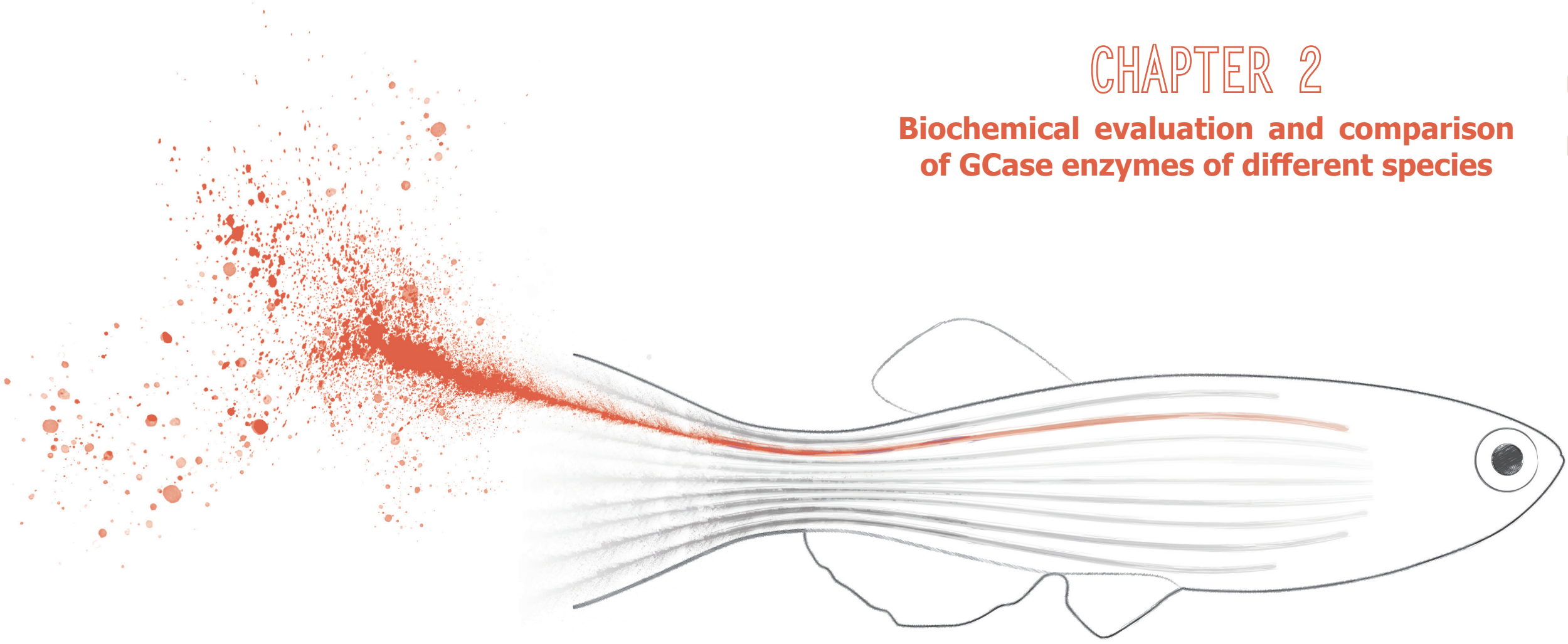

Abstract

The glycosphingolipid glucosylceramide (GlcCer) is degraded in the lysosome by the acid β-glucosidase glucocerebrosidase (GCase, official gene name *GBA*). A defect in GCase leads to the common lysosomal storage disorder Gaucher disease (GD). A complete deficiency of GCase in man and mouse is lethal due to trans-epidermal water loss, but fortuitously a complete *gba* knockout zebrafish is viable. In this chapter, a combination of biochemical assays and molecular modelling is used to study and compare features of GCase enzymes of different species, including man, zebrafish, frog and turtle. All GCase enzymes showed hydrolysis of the artificial substrate 4-methylumbelliferyl β-glucoside at an acidic pH optimum. Human GCase required either saposin C or sodium taurocholate at pH 5.2 for optimal activity, while zebrafish and frog GCase showed high hydrolysis rates at pH 4 without additives. Increased levels of endogenous GlcCer and the deacylated sphingoid base, glucosylsphingosine (GlcSph), in the *GBA*-depleted cells were corrected by expression of any of the GCase enzymes. Zebrafish GCase was remarkably active at low temperature (10 °C) when compared to the enzyme from other species. In sharp contrast to human and frog GCase, the zebrafish enzyme was unable to perform an *in vitro* transglucosylation reaction with cholesterol as acceptor. Zebrafish GCase showed slight glucose transfer to acceptor lipids composed of hydrophobic alkyl tails, such as ceramide, hypothesizing that cholesterol might not fit the catalytic pocket of zebrafish GCase. *In silico* comparisons of modelled structures of the various GCase enzymes, based on the established 3D-structure of the human enzyme, revealed divergent residues in the flexible loops of GCase. Attention was drawn to three residues with hydrophobic chains positioned close to the catalytic pocket of zebrafish GCase. However, zebrafish GCase with substitutions of these amino acids did not show improvement in transglucosylation. To further test the hypothesis it should be considered to swap entire loops among enzymes of different species.

Introduction

Lysosomal deficiency of the enzyme acid β-glucosidase (glucocerebrosidase, GCase, EC 3.2.1.45, family GH 30) hydrolysing glucosylceramide (GlcCer) constitutes the molecular basis of the lysosomal storage disorder Gaucher disease (GD)[1]. Newly synthesized GCase is translocated to the lumen of the endoplasmic reticulum (ER), where the N-terminal signal peptide is removed, four N-linked glycans are attached to asparagine residues and folding of the protein occurs[2,3]. Correctly folded protein becomes rapidly membrane-associated through binding to the lysosomal integral membrane protein 2 (LIMP2)[4-7]. In the Golgi apparatus the N-glycans of GCase are predominantly modified to complex-type structures and no mannose-6-phosphate moieties are generated[8]. Instead LIMP2 mediates transport of the GCase-LIMP2 complex to the lysosome[4-7]. The activator lipid-binding protein saposin C is required for optimal intralysosomal activity of GCase as is illustrated by findings that defects in saposin C causes symptoms similar to GD[9-11].

The structure of human GCase, as resolved by crystallography, shows three domains (**Figure 1A** and **B**)[12]. Domain I (residues 1-27 and 383-414; pink) consists of a 3-stranded antiparallel β-sheet followed by a loop, domain II (residues 30-75 and 431-497; green) of an 8-stranded β-barrel, resembling an immunoglobulin fold, and domain III (residues 76-381 and 416-430, blue) consists of the catalytic $(\beta/\alpha)_8$ triosephosphate isomerase (TIM) barrel, a domain conserved among glycosidases[12,13]. The catalytic residues are located in the TIM barrel with Glu 340 functioning as nucleophile and Glu 235 as acid/base. For a recent review see also Ben Bdira *et al.*[14].

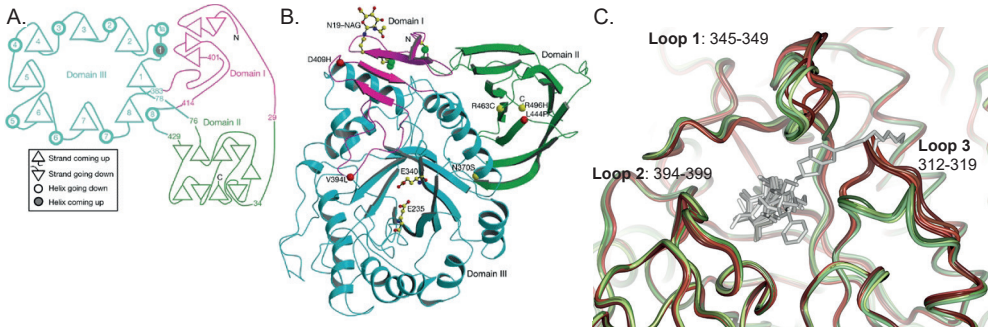

Figure 1 | Structural arrangement of human GCase
Two-dimensional topology **(A)** and 3D structure **(B)** of human GCase. Domain I is shown in pink, domain II in green and domain III in blue, with the numbers of α-helices and β-strands of domain III numbered according to the position in the sequence. Figure (A) and (B) are used from Dvir *et al.*[12]. **(C)** Conformational changes of loops 1, 2 and 3 from the inactive (red) to the active, ligand associated conformation (green), with modelled ligands in the active site (grey). Reported structures without ligand: PDB codes 1OGS, 2J25, 3GXD, 3GXI and 3GXM, and ligand associated: PDB codes 2XWE, 2V3D, 2V3E, 2NSK, 3GXF, 5LVX, 2VT0, 2WCG, 2XWD, 3RIK and 3RIL1OGS, 2J25, 3GXD, 3GXI and 3GXM.

Like other retaining glycosidases, GCase employs a Koshland double-displacement mechanism with Glu 340 performing a nucleophilic attack at the anomeric C1 carbon of the β-D-glucose moiety of GlcCer and Glu 235 protonating the oxygen of the glycosidic bond[15]. The aglycon is released and a covalent enzyme-glucose intermediate is formed. Insights into the reaction mechanism and covalent intermediate have been used to design covalent inhibitors for GCase inactivation and activity-based probes to visualize active GCase[16,17]. Next, Glu 235 activates a water molecule that acts as nucleophile and the glucose is released from the enzyme. In this second step, another suitable hydroxyl-containing molecule could serve as acceptor in a so-called transglucosylation reaction[18]. An established acceptor in the transreaction is cholesterol[18-20].

Three loops surround the catalytic active site: loop 1 (residues 345-349), loop 2 (residues 394-399) and loop 3 (residues 312-319), with amino acid numbering of human GCase based on the mature protein following the numbering described in previously published reports[13,21]. Crystallography and modelling studies point to a high flexibility of the three loops, adopting different conformations (**Figure 1C**)[13,22]. In the structure of the inactive enzyme the catalytic pocket seems small and suboptimal for substrate binding[13,22]. Loop 3 appears to change from an extended loop in the inactive enzyme conformation into a helical structure in the active GCase structure (**Figure 1C**)[22-24]. As a result, several residues change their hydrogen bonding interactions and together these conformational changes induce opening of the active site, which becomes wider and shallower. The structural changes are reviewed and visualized in detail in 2011 by Lieberman *et al.*[23].

The outer layer of the human skin, the stratum corneum, contains a large amount of active GCase molecules[25]. Complete absence of GCase is incompatible with terrestrial life in man and mice[26-28], while a complete GCase-deficient zebrafish is viable (chapter 6 and 7[29,30]). Therefore, the catalytic features of human and zebrafish GCase were studied and compared, as well as features of GCase enzymes from the amphibian *Xenopus laevis* (African clawed frog), and the reptile *Chrysemys picta belii* (western painted turtle, a freshwater turtle). These species were chosen in view of evolutionary aspects of the transition to terrestrial life and accompanying changes in skin composition. The outcome of the investigation is reported and discussed in this chapter.

Results

GCase of all tested species is catalytically active, although at different conditions

In order to allow a direct comparison of the GCase enzymes, CRISPR/Cas9 technology was used to generate human HEK293T cells lacking endogenous GCase activity. The various GCase enzymes were expressed under a CMV promoter in these *GBA* knockout (KO) HEK293T cells cultured at 37 °C. The comparison of the catalytic features of the different GCase enzymes was started by evaluating the enzymatic activity towards the artificial 4-methylumbelliferyl β-glucoside (4MU-β-Glc) substrate. All GCase enzymes were able to hydrolyse the substrate albeit at different conditions. Human GCase showed optimal hydrolysis at an acidic pH of 5.2 and required the additives Triton-X100 (Tx) and sodium taurocholate (Tc) for optimal hydrolysis, as described before[31] (**Figure 2A**, pink circles; closed and open for additives and no additives respectively). Activation of human GCase could also be obtained by addition of recombinant saposin C (SapC) and the negatively charged lipid phosphatidylserine (PS) (**Supplementary Figure 1A**). Turtle GCase also showed optimal hydrolysis around pH 5.2 and Tx/Tc slightly increased hydrolysis (**Figure 2A**, orange circles and inset). Both zebrafish and frog GCase did not require Tx/Tc and showed the highest hydrolytic activity around pH 4 (**Figure 2A**, blue and green circles for zebrafish and frog respectively). The K_m and V_{max} values for the 4MU-β-Glc substrate were determined for the different GCase enzymes. A high V_{max} of zebrafish and frog GCase was observed, while the low K_m of human GCase indicates a high affinity for 4MU-β-Glc as substrate.

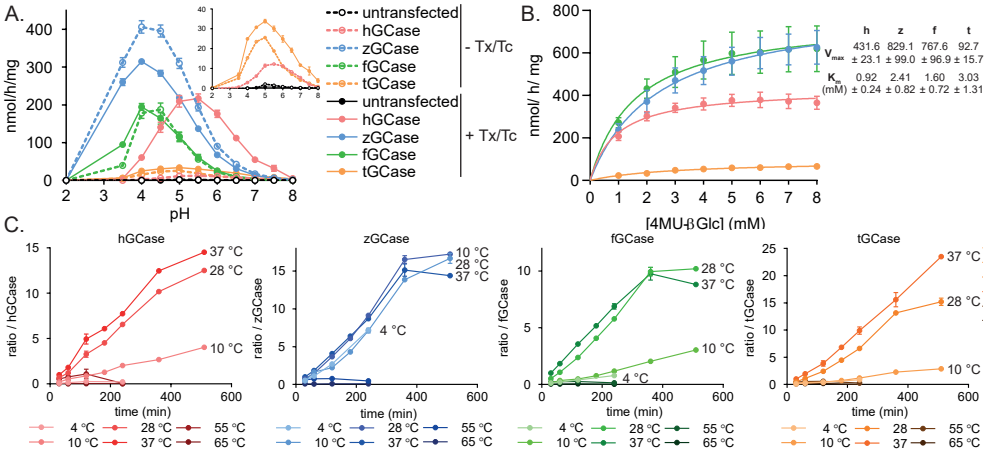

Figure 2 | Enzymatic activity of GCase enzymes towards 4MU-β-Glc

(A) Hydrolytic activity of untransfected cells (black) or cells over-expressing human (h, pink), zebrafish (z, blue), frog (f, green) and turtle (t, orange) GCase towards 4MU-β-Glc at different pH values without additives (open circles) or with additives (Triton-X100 (Tx) and Sodium Taurocholate (Tc); closed circles), incubated for 30 min at 37 °C. **(B)** Homogenate is incubated with different concentrations 4MU-β-Glc for 30 min at 37°C. V_{max} and K_m values are calculated using a Michaelis-Menten non-linear fit. **(C)** Activity of human GCase enzymes at different time points incubated at a range of temperatures. Activity is calculated as ratio compared to the activity at 30 min at 37 °C of that specific species. Activity is measured from 3 independent homogenate preparations for (A) and (B) and 2 independent homogenate preparations for (C). Data is depicted as mean ± SEM.

Next, hydrolysis was evaluated at different temperatures in time. The data is depicted as ratio compared to hydrolytic activity of the specific GCase at 37 °C and 30 min (**Figure 2C**). Zebrafish GCase showed relatively high activity over a broad temperature range from 4 °C to 37 °C, while the other enzymes showed 3-4 fold lower activity at 10 °C compared to 28 and 37 °C. The broad range of optimal temperatures for the zebrafish aligns with the poikilothermous nature of these animals, with their body temperature depending on the surrounding water.

A high potency of the GCase specific inhibitor, ME656[32], was observed for human and zebrafish GCase, with comparable IC_{50} values of 40 and 100 nM for human and zebrafish respectively (**Supplementary Figure 1B**).

Detection of active GCase using specific activity-based probe

The specific fluorescent activity-based probe for GCase was used to label all active enzyme. As expected, no band of approximately 50-60 kDa was observed in untransfected *GBA* KO cell homogenate. For human GCase, a broader band was observed around 55 kDa, corresponding to the differently glycosylated forms of GCase as described before (**Figure 3A,** top panel)[16]. ABP-labelled zebrafish, frog and turtle GCase was visualized around 55-60 kDa. An ABP-enzyme complex with lower molecular weight was apparent for all three GCase enzymes, which is likely a degradation product.

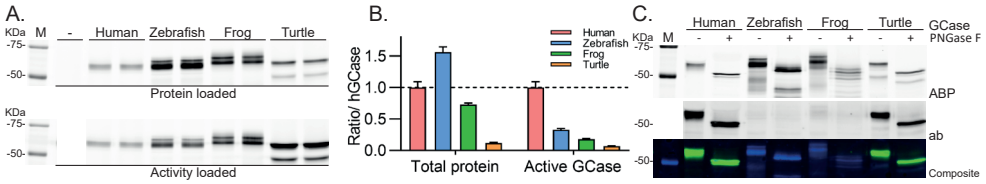

Figure 3 | Visualization of active GCase and total GCase

(A) Labeling of active GCase using a GCase specific ABP. Homogenates of untransfected cells (-) or cells over-expressing the different GCase enzymes were used and either loaded with similar amount of total protein (top panel) or similar activity towards 4MU-β-Glc (bottom panel). Two independent homogenate preparations were used. **(B)** Activity was calculated with respect to total protein levels (left) or the intensity of the GCase-ABP complex (right) quantified from (A) and depicted as ratio compared to hGCase. **(C)** Homogenate was labeled and subsequently deglycosylated using PNGase F (top panel; ABP). A commercial GCase specific primary antibody was used to visualize all GCase, both active and inactive (middle panel; ab). The composite figure (bottom panel) shows active GCase-ABP complex in blue and total GCase detected using anti-GCase in green.

Detection of zebrafish and frog GCase with ABP was good, however it was observed that the ratio of activity per unit of ABP-complex was lower compared to human GCase (**Figure 3A** and **B**). In contrast, expression and detection of turtle GCase was relatively low which corresponds to the observed low activity (**Figure 3A** and **B**).

Deglycosylation of the GCase enzymes by PNGase F removes all N-linked glycans and revealed a ABP-complex at a lower molecular weight of 50 kDa for all GCase enzymes (**Figure 3C**). The breakdown products described above were also apparent after deglycosylation. A commercially available antibody binding GCase could only visualize human and turtle GCase, while the ABP did not show species specificity (**Figure 3C**). The C-terminal part of human GCase was used to generate the commercial antibody (amino acids 478-497; underlined in **Figure 7**), a part of the protein with quite some variation between the different species.

Zebrafish GCase hardly shows transfer of glucose to a cholesterol acceptor

First, the optimal conditions for transglucosylation activity were determined for the different GCase enzymes. Cholesterol is a very apolar lipid, practically insoluble in water and aqueous solutions of bile salts or detergents are known to help solubilize cholesterol. Human GCase requires additives not only for optimal hydrolysis but also to perform optimal transglucosylation at pH 5.2 (**Figure 4A-C** and **Supplementary Figure 2**). Zebrafish GCase did not show significant GlcChol formation at the optimal conditions for hydrolysis (**Figure 4A-C**, -Tx/Tc). Addition of sodium taurocholate improved the amount of formed GlcChol, although decreased the hydrolytic activity compared to the condition without additives. The most interesting differences were found for frog GCase. This enzyme showed high enzymatic activity in the absence of additives, however no GlcChol was formed (**Figure 4A-C**). In the presence of Triton-X100, the hydrolytic activity remained similar and the amount of formed GlcChol is much higher compared to the condition without additives (**Figure 4A-C**). In contrast, addition of sodium taurocholate lowered both the amount of formed GlcChol and enzymatic activity towards 4MU-β-Glc. Similar findings for transglucosylation were found using the fluorescently labelled NBD-cholesterol as acceptor (**Supplementary Figure 3**). It is apparent from the investigation that addition of Triton-X100 and sodium taurocholate should be optimized for every GCase enzyme and experimental setting.

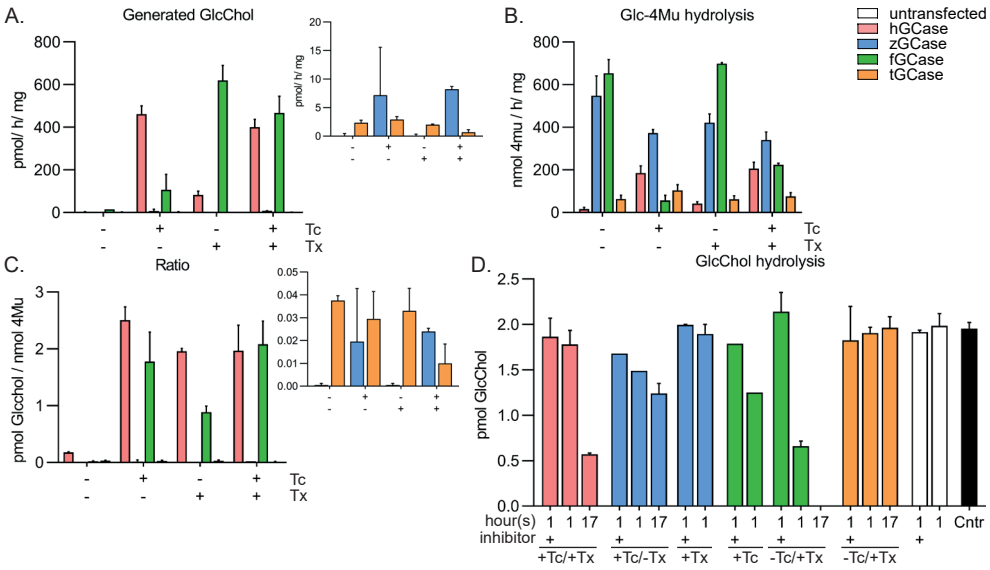

Figure 4 | *In vitro* generation and hydrolysis of GlcChol

(A-C) Homogenate (± 40 µg total protein) was incubated with 4MU-β-Glc as glucose donor and cholesterol as acceptor with different buffer conditions: without additives (-Tc/-Tx), with sodium taurocholate (+Tc/-Tx), with Triton-X100 (-Tc/+Tx) or with both additives (+Tc/+Tx). Formed GlcChol was measured using LC-MS/MS methods (A), while the hydrolytic activity was measured by 4MU detection (B). The ratio was calculated of pmol GlcChol formed for 1 nmol of hydrolysed 4MU-β-Glc (C). **(D)** Homogenate (± 40 µg) was pre-treated with vehicle or a GCase inhibitor for 30 min at 37 °C and subsequently incubated with 2 pmol GlcChol for 1 or 17 hours at 37 °C in the presence of Tx and/or Tc. For Cntr, lysis buffer was incubated with 2 pmol for 1 hour at 37 °C. Activity is measured from 2 independent homogenate preparations and data is depicted as mean ± SD.

Next, the ability to hydrolyse the formed GlcChol was evaluated (**Figure 4D**). GCase enzymes were incubated with a fixed amount of GlcChol for 1 hour or overnight (± 17 hours). To account for other enzymes and the different conditions, GCase homogenate was pre-blocked with a GCase inhibitor before addition of GlcChol. Both mock and turtle GCase did not show a significant decrease in GlcChol. Human GCase and zebrafish GCase did not show significant decrease in GlcChol after 1 hour of incubation, however both enzymes were able to hydrolyse part of the added GlcChol after overnight incubation. In contrast, frog GCase was able to hydrolyse most of the added GlcChol within 1 hour of incubation and no GlcChol was present after 17 hours of incubation.
Cholesterol, consisting of four hydrocarbon rings, is a bulky sterol, which might influence the positioning of the acceptor within the active site of the enzyme. Other NBD-lipids were tested as acceptor: sphingosine (Sph) and ceramide (Cer). Both human and frog GCase showed product formation when Sph and Cer were used (**Figure 5**). Turtle GCase, expressed at low amounts, did not show prominent GlcChol formation measured using the LC/MS-MS method and no NBD-GlcChol product could be detected using HPTLC as well. However, prominent NBD-Glc-product was visualized when Sph and Cer were used as acceptor. Zebrafish GCase did not show product formation when Chol was used as acceptor. When Cer was used as acceptor lipid, minor product formation was observed.

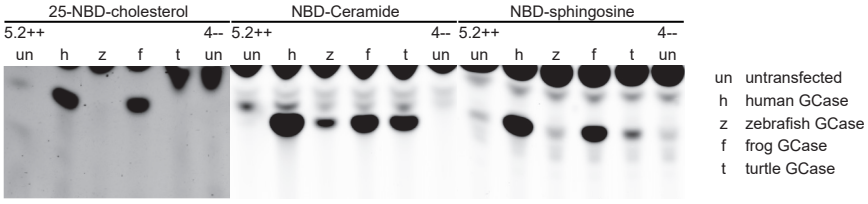

Figure 5 | *In-vitro* transglucosylation using different NBD-conjugated acceptor lipids
Homogenate (± 40 µg) of untransfected cells (un) or cells over-expressing human- (h), zebrafish- (z), frog- (f) or turtle- (t) GCase was incubated with donor (4MU-β-Glc) and different NBD-lipids for 1 hour at 37 °C with the optimal buffer conditions for every GCase enzyme. Lipids were separated on HPTLC silica gel plates using chloroform/ methanol (85:15, v/v) and visualized using fluorescent scanning of the plate.

Taken together, LC-MS/MS and HPTLC experiments indicate that human and frog are able to perform *in vitro* transglucosylation using multiple different types of acceptor lipids. Zebrafish GCase, on the other hand, is only able to use ceramide and possibly sphingosine. These findings lead to the hypothesis that a more flexible acceptor could be able to enter the active site of zebrafish GCase while a rigid, bulky acceptor lipid cannot.

GCase of all species is able to correct cellular glycosphingolipid abnormalities
The *GBA* KO HEK 293T cells show accumulation of the primary substrate GlcCer and the de-acylated sphingoid base, GlcSph (**Figure 6**; untransfected cells; white bar). These lipid abnormalities were corrected by the stable over-expression of either human, zebrafish, frog and turtle GCase (**Figure 6**). An increase in GlcSph was again observed when the cells were incubated with the GCase specific inhibitor ME656, indicating that the decrease of GlcSph can be attributed to the respective GCase. These findings confirm that the different GCase enzymes are both active and functional in their physiological environment, even though the *in vitro* activity of for example turtle GCase is much lower.

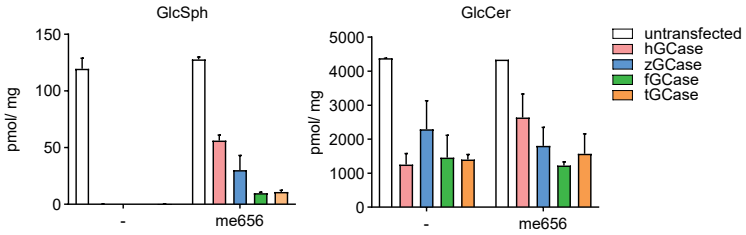

Figure 6 | Endogenous glycosphingolipid levels of cells expressing GCase enzymes of different species
GBA KO HEK273T cells over-expressing human-, zebrafish-, frog- or turtle GCase and *GBA* KO HEK293T control cells were incubated with vehicle (0.1% (v/v) DMSO) or a GCase inhibitor (100 nM me656, 0.1% (v/v) DMSO) for 36 hours. GlcSph and GlcCer levels were measured and calculated in pmol/mg total protein. Two independent cell experiments were performed and data is depicted as mean ± SD.

Alignment and homology models indicate differences in GCase enzymes

The observed differences in enzymatic activity and transglucosylation might be related to structural differences between the GCase enzymes of different species. Two approaches were used to compare the amino acid sequences of the different GCase enzymes. First, the mature amino acid sequences of human, zebrafish, frog and turtle GCase were aligned using Clustal Omega and important residues highlighted (**Figure 7**). In addition, simple homology models were generated of the zebrafish, frog and turtle structures with SwissModel, based on the established 3D-structure of the human enzyme (PDB code 2XWE), in order to evaluate the position of aberrant residues (**Figure 8**). Conserved and aberrant residues located in the catalytic pocked and the three flexible loops are summarized in **Table 1**.

In the alignment of the primary sequences, the nucleophilic and acid/base glutamatic acid residues are conserved (**Figure 7**; Nucleophile (N) and Acid/Base (a/b), arrows) as well as the four cysteine residues forming disulfide bridges are conserved in all species (**Figure 7**, orange). The four N-glycosylation sites with reported glycans in human GCase[2,3] are not all conserved in the different GCase of other species (**Figure 7**; Asn 19, Asn 59, Asn 146 and Asn 270, dark green). *In silico* prediction of N-glycosylation sites showed only 3 predicted sites for zebrafish, 4 sites for frog and 3 sites for turtle GCase (**Figure 7**, dark and light green). Results of the PNGase F treatment (**Figure 3C**) only indicated that GCase of zebrafish, frog and turtle indeed have N-linked glycans, although it is not known how many they have. Properly folded GCase is recognized by LIMP2 and transported as LIMP2-GCase complex to the lysosome. Helix 1a and 1b (residues Thr 86- Leu 96 and Pro 99 – Ser 110) and helix 2 (Pro 150 – Arg 168) of GCase were found important for LIMP2 binding (underlined in **Figure 7**)[5]. These helix motifs displayed hydrophobic patches interacting with LIMP2 (yellow highlight in **Figure 7**). These hydrophobic patches of human GCase are conserved in the amino acid sequences of the other GCase enzymes. This could explain the functional lysosomal localisation of the different enzymes in the human *GBA*-KO cells which would imply interaction of the non-mammalian GCase with human LIMP2.

Several residues of prevalent GD mutations are conserved not only in mammals, but also in the GCase sequences studied in this chapter (**Figure 7**, red)[33]. The residues leading to D409H, R463C and R496H are conserved in zebrafish, frog and turtle GCase. The polar uncharged Asn 370, leading to the prevalent N370S mutations is present in turtle GCase, however a negatively charged Asp residue is present at this position in zebrafish and frog GCase. The human Leu 444, leading to the L444P mutation, is present in the zebrafish and frog protein sequence, while another hydrophobic residue, Met, is present at this position in the turtle GCase sequence.

Table 1 | Divergent residues in zebrafish, frog and turtle GCase compared to human GCase are depicted in orange and bold. Data was obtained from the alignment of the mature amino acid sequence using Clustal Omega and the generated homology models, based on the reported 3D-structure of human GCase.

	Human	Zebrafish	Frog	Turtle	
Loop 3	W312	W314	W313	W312	
"	Y313	Y314	Y314	Y313	
"	L314	**F316**	L315	L314	
"	D315	D317	D316	D315	
"	F316	**R318**	**A317**	F316	
"	L317	L319	I318	I317	
"	A318	**V320**	**V319**	A318	
"	P319	P321	P320	P319	
	C342	C344	C343	C342	
	V343	**A345**	**T344**	**T343**	
	G344	G346	G345	G344	
Loop 1	S345	**W347**	**F346**	S345	
"	K346	**S348**	**T347**	**H346**	
"	F347	**P349**	**P349**	F347	
"	W348	**V350**	W349	W348	
"	E349	**D351**	**N350**	E349	
	Q350	**R352**	**K351**	**R350**	
Loop 2	V394	V396	V395	V394	
"	R395	**K397**	**E396**	**Q395**	
"	N396	N398	N397	N396	
"	F397	F399	**N398**	**L397**	
"	V398	V400	V399	V398	
"	D399	D401	D400	D399	
Acid/base	E235	E237	E236	E235	
Nucleophile	E340	E342	E341	E340	
	N370	**D372**	**D371**	N370	N370S mutation
	D409	D411	D410	D409	D409H mutation
	L444	L446	L446	**M447**	L444P mutation
	R463	R465	R465	R466	R463C mutation
	R496	R498	R498	R499	R496H mutation

In silico comparisons of modelled GCase structures

Besides the nucleophile and acid/base glutamic acid residues, several residues line the catalytic pocket of human GCase, which were apparent in established 3D-structures[22,23,34,35]. Most of these residues are conserved in the zebrafish, frog and turtle GCase as shown by the homology model (**Figure 8A**), including Arg 120, Asp 127, Phe 128, Trp 179, Asn 234, Tyr 244, Phe 246, Tyr 313, Cys 342, Ser 345, Trp 381, Asn 396, Phe 397, and Val 398 of human GCase. Two exceptions were observed: the polar side chain of Ser 345 is replaced by a hydrophobic side chain in the zebrafish and frog (Trp and Phe respectively), while the hydrophobic side chain of Phe 397 is present in the zebrafish but is replaced by the hydrophobic, small side chain of Leu in turtle and the polar side chain of Asn in frog (**Figure 8A** and **Table 1**).

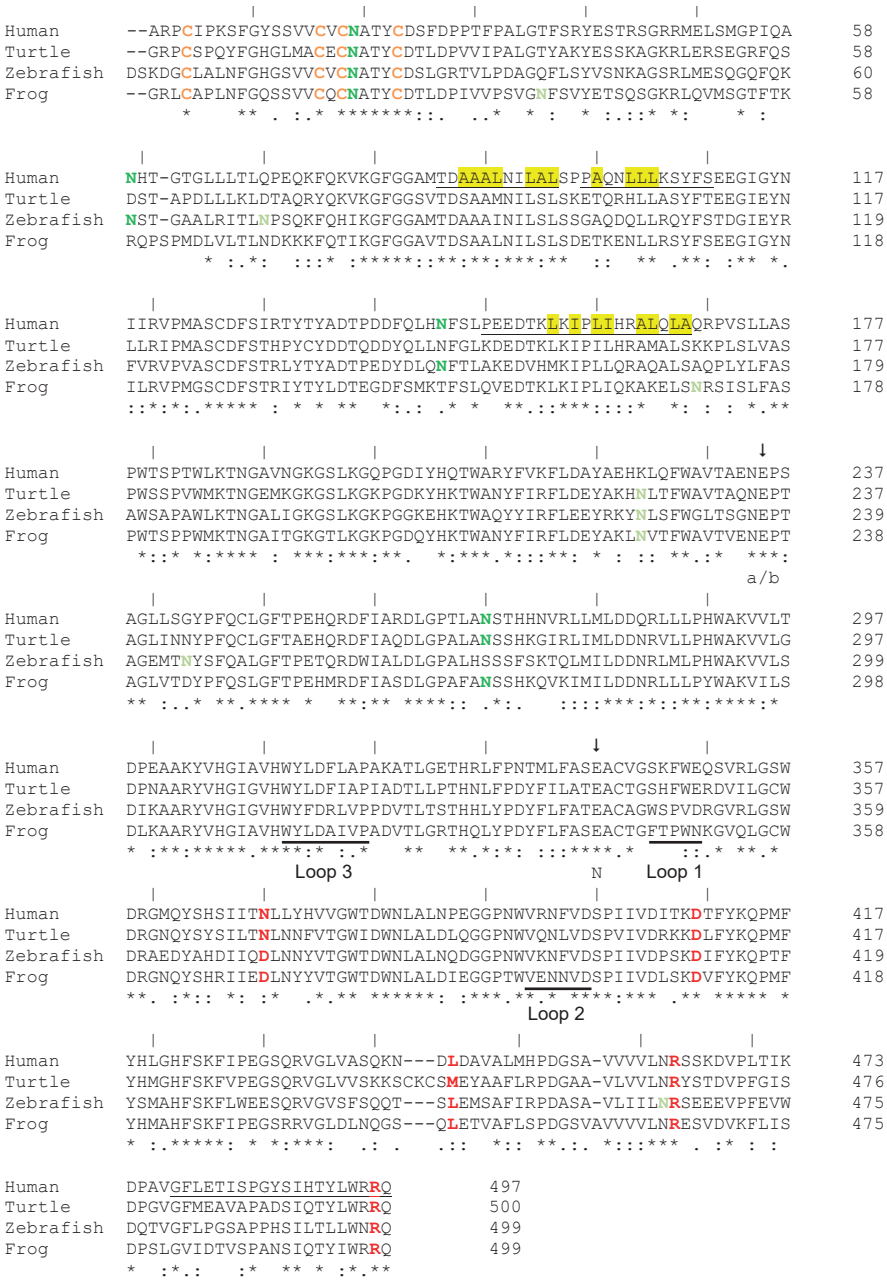

Figure 7 | Alignment of the amino acid sequence of GCase of the different species

Alignment of the mature amino acid sequences of human-, zebrafish-, frog- and turtle GCase using Clustal Omega. Alignments showed amino acid identities of 57.8 % for zebrafish, 63.5 % for frog and 64.6 % for turtle GCase compared to human GCase. Important residues in the human GCase sequence are depicted as follows: both the nucleophile (N) and acid/base (a/b) are indicated with an arrow, the cysteine residues forming disulphide bridges in human GCase are depicted in orange, N-glycosylation sites of human GCase in dark green and the predicted N-glycosylation sites in light green. The predicted antibody binding site of Figure 3C is underlined at the C-terminal end, while the N-terminal human LIMP2 binding site is underlined and hydrophobic patches are highlighted in yellow. Prevalent, clinically relevant mutations in GD are depicted in red. * = conserved residue, : = strongly similar residue, . = weakly similar residue, | = every 10th residue of the human GCase

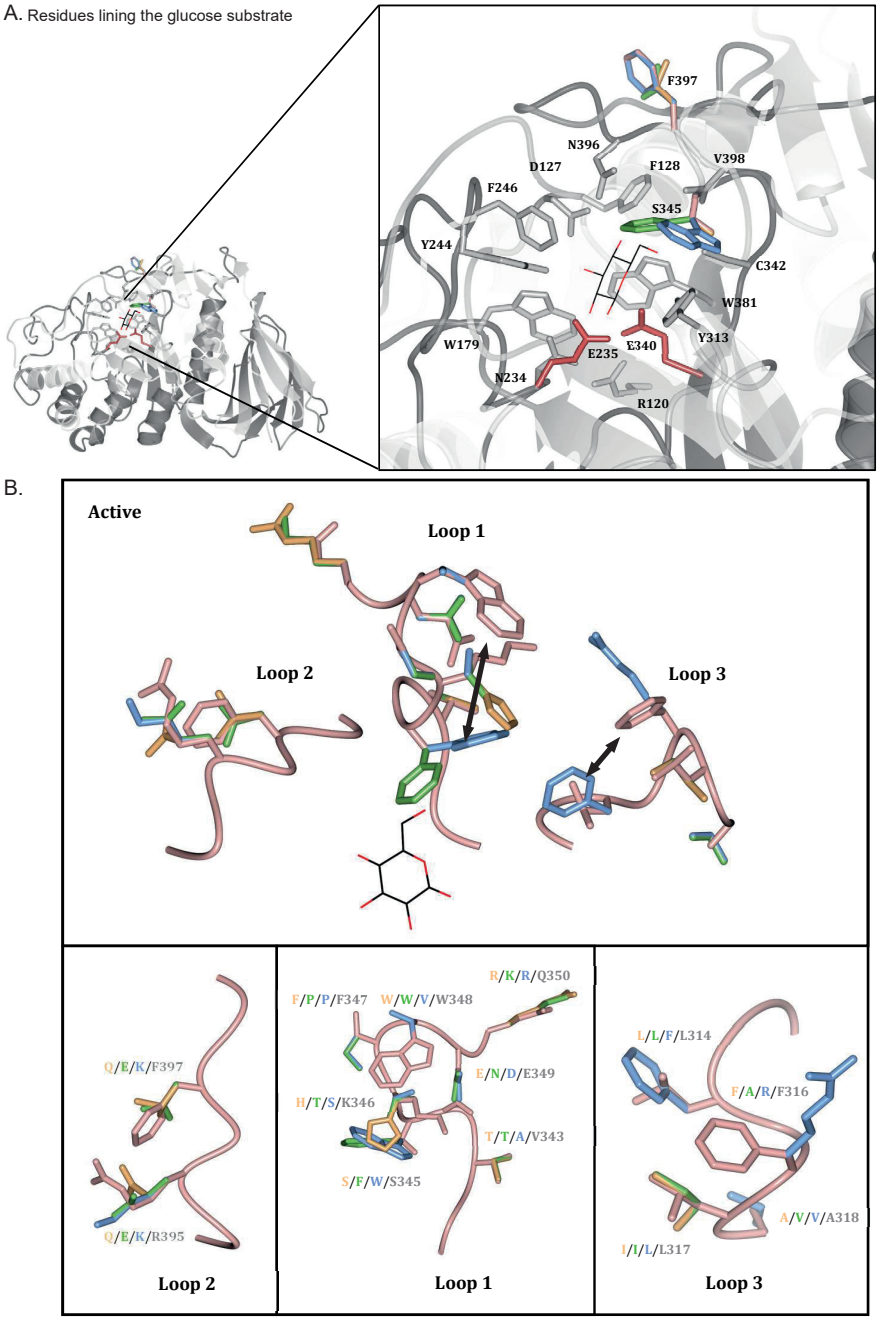

Figure 8 | *In silico* comparison of homology GCase models
Homology models were generated of the zebrafish, frog and turtle structures with Swissmodel, based on the reported 3D-structure of human GCase (PDB code 2XWE[36]). **(A)** Glucose-lining residues. Similar residues with respect to the human structure are depicted in grey, the nucleophilic Glu 340 and acid/base Glu 235 in red, while aberrant residues are visualized with the respective color for human (pink), zebrafish (blue), frog (green) or turtle (orange) residues. **(B)** Loops 1, 2 and 3 in the active conformation of human GCase with residues of human (pink/grey), zebrafish (blue), frog (green) and turtle (orange) GCase. Divergent residues at the modelled position are given in the respective color in the lower panel.

Mutagenesis of selected amino acids in zebrafish GCase does not changes its features

Established 3D-structures of GCase revealed different conformations of loops 1, 2 and 3 in the inactive- versus the active, ligand associated human GCase structures. Interactions of specific residues in these loops are thought to facilitate the closed conformation of the inactive, unbound structure, while conformational changes of the loops is suggested to open the active site[13,23]. Several residues are different in the modelled loops 1, 2 and 3 of the zebrafish, frog and turtle structures (**Figure 8B**). The most intriguing differences are between the human and zebrafish sequences. In the homology model, Trp 348 of loop 1 in human GCase is replaced in the zebrafish sequence by a Val, while a Trp with bulky side chain of zebrafish GCase substitutes human Ser 345. In loop 3, Phe 316 in human GCase is replaced in zebrafish by an Arg residue, while Leu 314 is replaced by a Phe residue. These *in silico* models suggest that the hydrophobic side chains of Trp and Phe are present in the zebrafish structure, albeit positioned closer to the catalytic pocket (depicted in **Figure 8B** by the arrows).

It was hypothesized that these substitutions might impair entrance of the bulky sterol acceptor. In order to test this hypothesis, three different mutations of the zebrafish GCase were generated and evaluated: 1) F316L, 2) W347S, and 3) a double mutation of F316L + R318F. GCase enzymes with these mutations were transiently expressed in the *GBA* KO cells and the catalytic features were determined in a pilot experiment. No change in pH optimum of the hydrolysis reaction was observed nor an improvement in GlcChol formation. A decrease in activity of the W347S zebrafish GCase was observed, however transient transfection was only performed once and this effect might be due to biological variation. Taken together, these single- and double amino acid substitutions did not validate the hypothesis of improved access of cholesterol in the zebrafish enzyme. To test further this hypothesis, future endeavours could focus on swapping the entire candidate loop 1 or 3 among the different species.

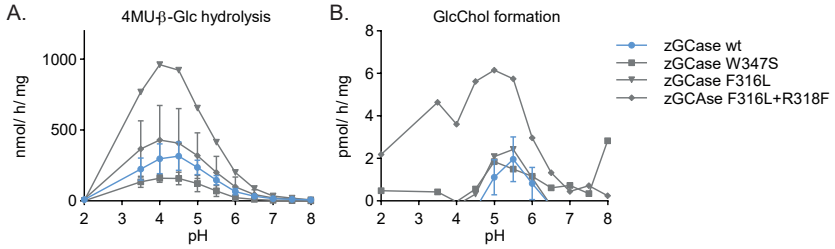

Figure 9 | Enzymatic activity and GlcChol formation of zebrafish GCase variants

(A) Hydrolytic activity of zebrafish GCase WT and GCase variants (W347S, F316L and F316L+R318F) towards 4MU-β-Glc at different pH values without additives incubated for 30 min at 37 °C. **(B)** Homogenates (± 40 µg total protein) were incubated with 4MU-β-Glc as glucose donor and cholesterol as acceptor at different pH with 0.1% (w/v) BSA and 0.1% (v/v) Triton-X100. Formed GlcChol was measured using LC-MS/MS methods. Data is depicted from a single pilot experiment (no error bars) or biological duplicate with mean ± SEM.

Discussion

Zebrafish are an emerging and attractive research model to evaluate the potency and selectivity of small molecules and to study genetic disorders such as the lysosomal storage disease GD. The aim of present study was to evaluate whether the highly homologous zebrafish GCase enzyme has similar features to its human counterpart. In parallel, GCase enzymes of an amphibian (*Xenopus laevis*, frog) and reptile (*Chrysemys picta bellii*, turtle) were studied. The zebrafish, frog and turtle GCase enzymes were highly homologous to the human counterpart, with an amino acid identity of 57.8 % for zebrafish, 63.5 % for frog and 64.6 % for turtle GCase. In particular residues lining the catalytic pocked showed high conservation among the different GCase sequences.

The coding sequences of the different GCase enzymes were cloned into a mammalian expression vector and stably expressed in *GBA* KO human embryonic kidney (HEK293T) cells, generated by means of CRISPR/Cas9. ABP-labelling revealed GCase-labelled proteins at comparable molecular weight as well as the presence of N-linked glycans in all enzymes. The enzymatic features of zebrafish, frog and turtle GCase were quite comparable to the human GCase. All four enzymes were active *in vitro* towards the artificial substrate 4MU-β-Glc at an acid pH optimum and were able to correct endogenous accumulated GlcCer and GlcSph in the *GBA* KO HEK293T cells. These findings implied that newly synthesized GCase enzymes of zebrafish, frog and turtle are able to interact *in situ* with the endogenous human LIMP2 protein. In similar manner, it can be argued that the non-mammalian GCase enzymes are able to interact *in situ* with human Saposin C. However, caution is warranted since over-expression of GCase as such might be sufficient to correct the increased GlcCer and GlcSph lipids.

Of note, comparable enzymatic features were noted when the non-lysosomal β-glucosidase Gba2 of the zebrafish was compared to its human counterpart[37]. In addition, in *vivo* treatment of developing zebrafish larvae with inhibitors of GCase, Gba2 or glucosylceramide synthase (GCS) showed aberrant glycosphingolipid levels similar to treatments of mammalian systems as discussed in chapter 5[32,38-40]. Altogether these data suggest that GlcCer metabolism as well as enzymes responsible for synthesis and catabolism are similar in zebrafish as compared to mammals.

Although all GCase enzymes were found to be active, several differences were also observed. **Table 2** summarizes the most relevant observations in this respect. First, it became apparent that human GCase requires additives, either Triton-X100 and sodium taurocholate or recombinant Saposin C with phosphatidylserine, for maximal activity. Both zebrafish and frog GCase require no additives for maximal enzymatic activity towards 4MU-β-Glc and show a lower pH optimum of pH 4. A striking difference between zebrafish GCase and the other studied GCases is the high activity of the former enzyme at low temperature. Sharply contrasting with human GCase, zebrafish enzyme was at 4 and 10 °C as active as at 28 and 37 °C.

Another major difference between zebrafish and human GCase is the inability of the former to catalyse a transglucosylation reaction in vitro using cholesterol as acceptor. Frog GCase is able to efficiently transfer the glucose from a glucose donor to a cholesterol

acceptor, as human GCase[18]. GlcChol formation by frog GCase was low in the absence of additives. Transglucosylation activity increased when Triton-X100 was added, but prohibited by sodium taurocholate, sharply contrasting human GCase[31]. It is of interest to stress that zebrafish GCase showed *in vitro* transglucosylation activity when a more flexible NBD-lipid like ceramide was used as acceptor.

Table 2 | Overview of the findings regarding *in vitro* hydrolysis and transglucosylation as well as *in situ* correction. 0 = no stimulation, ND = not determined, NR = not reproducible, SA/ABP = specific activity / ABP-complex.

	Hydrolysis					Transglucosylation			*In situ*
Enzyme	Tc/Tx stimulation	SapC simulation	pH optimum	SA/ABP	10/37 °C	Ability?	Additives?	GlcChol hydrolysis	GlcCer/GlcSph correction
Human	++	++	5.2	++	--	yes	Tx/Tc	++	Yes
Turtle	(+)	ND	5.2	--	--	NR	NR	NR	Yes
Frog	0	ND	4.0	-	--	yes	Tx	+++	Yes
Zebrafish	0	0	4.0	-	++	no	(Tc)	+	Yes

The combined findings raised the possibility that zebrafish GCase is in a more active fold permanently, independent of temperature and additives, as compared to human GCase. This more 'rigid' conformation of zebrafish GCase may as downside limit the enzyme's ability to transfer glucose to structurally rigid acceptors like cholesterol. Of note, zebrafish GCase shows hydrolytic activity towards GlcChol that is formed in cells by the non-lysosomal GBA2 (see Chapters 5 and 7).

It was hypothesized that specific side chains of the zebrafish GCase might impair entrance of a bulky acceptor, like cholesterol, for the transglucosylation reaction. *In silico* comparison of the modelled structures revealed that most of the glucose-lining residues of the catalytic pocked were conserved among the three GCase enzymes compared to human GCase, while aberrant residues were apparent in flexible loops 1, 2 and 3. In particular, substitutions of human Leu 314 and Phe 316 of loop 3 and Ser 345 of loop 1 were noticed in the zebrafish GCase enzyme and it appeared that the hydrophobic side chains were positioned closer to the catalytic pocket of the zebrafish enzyme. Interestingly, a recent patent filed by Amicus describes a mutated human GCase with the double amino acid substitution F316A and L317F located in loop 3, showing increased catalytic activity and a doubled half-life at pH 7.5 compared to WT human GCase[41]. It was considered that specific side-chain conformations could form a more ordered region near the catalytic pocket and might be less prone to unfolding at neutral pH. Human Phe 316 is among one of the contrasting residues in the zebrafish and frog GCase enzymes. In addition, it has been found that the structural stability of recombinant GCase improves at acidic pH, showing an increased half-life, higher melting temperature and lower sensitivity to tryptic digestion[42]. Binding of (semi-)covalent inhibitors increased the structural stability even further. Therefore, it might be informative to study the structural stability of the GCase enzymes of different species in order to evaluate the structural compactness and susceptibility for proteolytic cleavage of the different enzymes.

A detailed comparison of human and zebrafish GCase, with parallel comparisons of frog and turtle GCase, was chosen in view of evolutionary aspects and accompanying changes in skin composition associated with the transition to terrestrial life. GCase sequences of several other non-mammalian species are known and alignment in combination with simple

modelling indicates that a lower number of divergent residues are present in loops 1, 2 and 3 of reptiles and birds compared to the fish and amphibian species (**Supplementary Table 1**: python, goose, crocodile, dolphin and mouse GCase). Loop 3 is entirely conserved in reptiles, birds and mammals, but not in zebrafish and frog. This loop 3 shows the largest conformational change based on the established 3D-structures of human GCase[22-24]. Studying the *in vitro* hydrolysis, transglucosylation and stability of these additional GCase enzymes could provide more information on the impact of divergent residues in the GCase enzymes. Of note, efforts have been made to express the GCase enzyme of the python, exactly as performed for the other GCase enzymes. Surprisingly, no enzymatic activity and no ABP-labelled band could be found for python GCase (data not shown). A possible explanation for the complete absence of expression in case of python and low expression of turtle GCase might be the utilized endogenous signal peptide of the respective GCase. In future experiments the predicted signal peptide sequence could be replaced by the human signal peptide sequence in order to evaluate the influence of the endogenous signal peptide and possibly improve expression.

As final part of this study, site-directed mutagenesis of the zebrafish GCase enzyme was performed to test the hypothesis of impaired access of cholesterol by the residues with hydrophobic side chains. The zebrafish GCase variants with rationalized single- and double amino acid substitutions did not impact the pH optimum or GlcChol formation. Swapping the entire candidate loop 1 or 3 among the different species might be a more productive approach for evaluating the influence of these loops on GlcChol formation. In addition, crystallization of the zebrafish GCase enzyme could be very informative, as present *in silico* comparisons are limited by the simple molecular modelling of divergent residues. Crystallization and subsequent comparison of the zebrafish GCase structures with human counterparts could reveal real differences in the 3D-structure of GCase.

In conclusion, the zebrafish GCase enzyme shows comparable hydrolytic activity to human GCase, but markedly differs in ability to transglucosylate and the influence of temperature on enzymatic activity. The molecular basis for these difference warrants further investigation by detailed studies of the structures of the GCases.

Acknowledgments

Daniel van Geest is kindly acknowledged for his extensive contribution to this study by performing part of the enzymatic assay as well as generation of the zebrafish GCase variants and subsequent pilot experiments. Marc Hazeu is acknowledged for the expression and purification of recombinant human saposin C.

Supplementary information

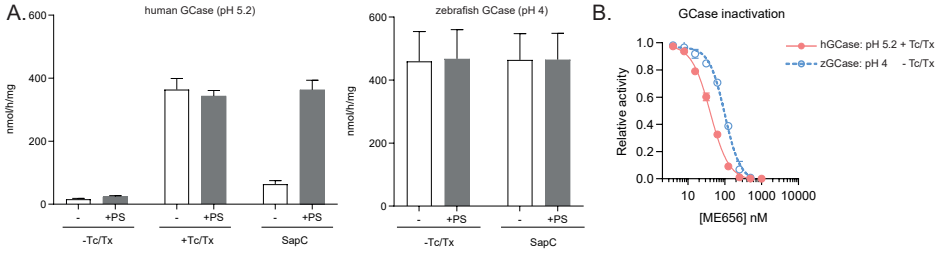

Supplementary Figure 1
(A) Enzymatic activity towards 4MU-β-Glc in the presence of the additives Triton-X100 (Tx) and sodium taurocholate (Tc) or Saposin C with or without addition of phosphatidylserine (PS) of human GCase at pH 5.2 (left) or zebrafish GCase at pH 4 (right). **(B)** IC_{50} curves of the inactivation of human (pink) or zebrafish (blue) GCase by the GCase specific inhibitor, ME656. Activity is measured from 3 independent homogenate preparations for (A) and in technical duplicate for (B). Data is depicted as mean ± SD.

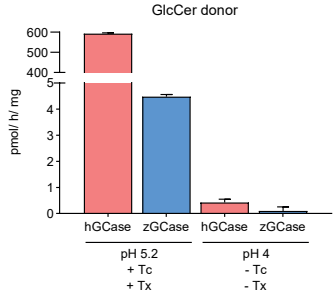

Supplementary Figure 2 | Transglucosylation with GlcCer as donor
Cell homogenate (± 40 µg) expressing human or zebrafish GCase was incubated with GlcCer d18:1/18:1 as glucose donor and cholesterol as acceptor in buffer of pH 4 without additives (-Tc/-Tx) or buffer of pH 5.2 with Triton-X100 and sodium taurocholate (+Tc/+Tx) for 5 hours at 37 °C. Formed GlcChol was measured using LC-MS/MS techniques in technical duplicate.

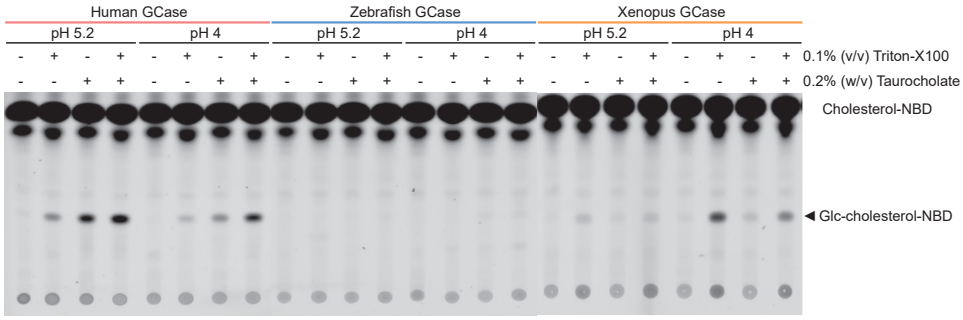

Supplementary Figure 3 | Effect of Triton-X100 and Sodium Taurocholate on transglucosylation with NBD-Chol
Cell homogenate (± 40 µg) expressing human, zebrafish or frog GCase was incubated with 4MU-β-Glc as glucose donor and NBD-cholesterol as acceptor in McIlvaine buffer of pH 4 or pH 5.2 supplement with Triton-X100 and/or Sodium Taurocholate and incubated for 1 h at 37 °C. Formed NBD-GlcChol was detected using fluorescent scanning of the separated lipids on a HPTLC plate using $CHCl_3$/MeOH (80:20) as eluents.

Supplementary Table 1 | Comparison of residue substitutions of human, zebrafish, frog, turtle GCase and GCase enzymes of additional species: python, goose, saltwater crocodile, freshwater crocodile, dolphin and mouse GCase. Data was obtained from the alignment of the mature amino acid sequence using Clustal Omega and the generated homology models, based on the reported 3D-structure of human GCase. Different residues compared to the human enzyme are depicted in orange and bold.

	Human	Zebrafish	Frog	Turtle	Python	Goose	Crocodile (salt)	Crocodile (fresh)	Dolphin	Mouse
Loop 3	W312	W314	W313	W312	W312	W312	W312	W312	W312	W311
"	Y313	Y314	Y314	Y313	Y313	Y313	Y313	Y313	Y313	Y312
"	L314	**F316**	L315	L314	L314	L314	L314	L314	L314	**M313**
"	D315	D317	D316	D315	D315	D315	D315	D315	D315	D314
"	F316	**R318**	**A317**	F316	F316	F316	F316	F316	F316	F315
"	L317	L319	**I318**	**I317**	L317	**I317**	L317	L317	L317	L316
"	A318	**V320**	**V319**	A318	A318	**G318**	A318	A318	A318	A317
"	P319	P321	P320	P319	P319	P319	P319	P319	P319	P318
	C342	C344	C343	C342	**S342**	C342	**S345**	C342	C342	C341
	V343	**A345**	**T344**	**T343**	**T343**	**I343**	**A346**	V343	V343	V342
	G344	G346	G345	G344	G344	G344	G347	G344	G344	G343
Loop 1	S345	**W347**	**F346**	S345	S345	**A345**	S348	S345	S345	S344
"	K346	**S348**	**T347**	**H346**	**Y346**	**H346**	**Y349**	K346	K346	K345
"	F347	**P349**	**P349**	F347	F347	F347	F350	F347	F347	F346
"	W348	**V350**	W349	W348	W348	W348	W351	W348	W348	W347
"	E349	**D351**	**N350**	E349	E349	E349	E352	E349	E349	E348
	Q350	**R352**	**K351**	**R350**	**P350**	**R350**	**P353**	Q350	Q350	Q349
Loop 2	V394	V396	V395	V394	**S394**	V394	**S397**	V394	V394	V393
"	R395	**K397**	**E396**	**Q395**	**K395**	**K395**	**K398**	**K395**	R395	R394
"	N396	N398	N397	N396	N396	N396	N399	N396	N396	N395
"	F397	F399	**N398**	**L397**	**Y397**	**Y397**	**Y400**	F397	F397	F396
"	V398	V400	V399	V398	V398	V398	V401	V398	V398	V397
"	D399	D401	D400	D399	D399	D399	D402	D399	D399	D398
Acid/base	E235	E237	E236	E235	E235	E235	E238	E235	E235	E234
Nucleophile	E340	E342	E341	E340	E340	E340	E343	E340	E340	E339

Experimental procedures

Chemicals and reagents - The GCase specific inhibitor (ME656), ABP (ME569) and $^{13}C_6$-GlcChol internal standard were synthesized as described earlier[16,18,32]. Chemicals were obtained from Sigma-Aldrich (St. Louis, MO, USA) if not otherwise indicated. Primers (**Supplementary Table 2**) were ordered from Integrated DNA technologies (IDT; Coralville, USA) without additional purification.

Cloning of the coding sequence of *gba* from different species - Design of cloning primers and plasmids containing the coding sequence of *gba* of different species were based on NCBI sequences NM_000157.4 (human), XM_682379.7 (zebrafish), XM_018229065.1 (frog) and XM_005280678.2 (turtle). The coding regions of human and zebrafish GCase were amplified using Phusion HighFidelity PCR mastermix (Thermo Fisher Scientific, Waltham, USA) using the primers given in **Supplementary Table 2**. Fragments of human and zebrafish *GBA* were cloned into the pDONR vector using GATEWAY™ recombination cloning technology (BP reaction, Thermo Fisher) according to the manufacturer's instruction and subsequently shuttled to a pDEST-zeo expression vector (derived by replacing the neomycin selection marker with a zeomycin selection marker) using the LR reaction.
Plasmids including the coding sequences of frog and turtle with flanking LR sequences and cloned into the pUC57-Kan vector backbone, were ordered from Baseclear (Leiden, the Netherlands). A LR reaction was performed shuttling the respective *gba* sequence to the pDEST-zeo expression vector.
For CRISRP/Cas9 mediated *GBA* knockouts of HEK293T cells, sgRNA guides given in **Supplementary Table 2** were cloned into the BbsI restriction site of the px330-U6-chimeric_BB-CB-hSpCas9 (Addgene plasmid #42230). All plasmids were isolated from transformed DH5α cells using a plasmid isolation kit (Qiaprep spin Miniprep kit; Qiagen, Hilden, Germany) and sequenced.
Site-directed mutagenesis – Point mutations were introduced in the zebrafish GCase pDONR vector using the QuickChange Lightning Site-Directed Mutagenesis Kit (Agilent, Santa Clara, USA) according to the suppliers protocol with the primers given in **Supplementary Table 2**. The double F316L+R318F mutation was generated by mutating the pDONR vector of the zebrafish GCase variant with the F316L mutation. The pDONR vectors were sequenced before shuttling the GCase encoding sequences to the pDEST-zeo expression vector.

Supplementary Table 2 | List of oligonucleotide sequences.

Primer	Sequence (5' -3')	Purpose
Human *GBA* F	GGGGACAAGTTTGTACAAAAAAGCAGGCTccACCACCATGGAGTTTTCAAGTCCTTCC	Gateway cloning
Human *GBA* R	GGGGACCACTTTGTACAAGAAAGCTGGGTTCATCACTGGCGACGCCACAGGTA	Gateway cloning
Zebrafish *gba* F	GGGGACAAGTTTGTACAAAAAAGCAGGCTACCACCATGAGAGAAACGGCTCTTTTTATTC	Gateway cloning
Zebrafish *gba* R	GGGGACCACTTTGTACAAGAAAGCTGGGTcTTACTGTCTGTTCCACAGTAGTG	Gateway cloning
Hu *GBA* sgRNA F	CACCGCGCTATGAGAGTACACGCAG	sgRNA for px330
Hu *GBA* sgRNA R	AAACCTGCGTGTACTCTCATAGCGC	sgRNA for px330
Zf GCase W347S F	gaggcatgcgctgggtCgagtccagtggatcgt	Mutagenesis
Zf GCase W347S R	acgatccactggactcGacccagcgcatgcctc	Mutagenesis
Zf GCase F316L F	gcattggtgttcactggtatttGgatcgccttgtgcc	Mutagenesis
Zf GCase F316L R	ggcacaaggcgatcCaaataccagtgaacaccaatgc	Mutagenesis
Zf GCase R318F F	attggtgttcactggtatttGgatTTccttgtgccgcctg	Mutagenesis
Zf GCase R318F R	caggcggcacaaggAAatcCaaataccagtgaacaccaat	Mutagenesis

Cell culture and transfection - HEK293T (CRL-3216) were purchased from ATCC (Manassas, VA, USA) and cultured at 37 °C and 5% CO_2 in DMEM medium, supplied with 10% (v/v) FCS, 0.1% (w/v) penicillin/streptomycin, and 1% (v/v) Glutamax. *GBA* KO cells were obtained by CRISPR/Cas9 technology by transfecting HEK293T cells seeded in 6-well plates with the px330-*GBA* plasmid in combination with Fugene 6 (Roche; Basel, Switzerland) in a ratio of Fugene:DNA of 3:1. After 72 hours, cells were diluted to approximately 0.5 cell/well, seeded in 96-well plates and individual clones were cultured over the next weeks. GCase activity was determined of the single cell clones, as described below, and only clones without residual activity were maintained. *GBA* KO clone 35 was verified using Sanger sequencing and used for experiments, subsequently called *GBA* KO cells. *GBA* KO cells were transfected using PEI and the pDEST-zeo-*gba* construct (PEI/DNA: 3/1 (w/w)). Cells expressing the

protein of interest were selected by sub-culturing the cells in medium supplemented with 200 µg/mL Zeomycin for at least 5 passages starting 24 hours after transfection. For transient expression, cells were transfected, as described above, for 72 hours before harvesting. Cells were harvested in PBS and washed twice with PBS. Cell pellets were stored at -80 °C until use.
Homogenate preparation - Cells were resuspended in 25mM potassium phosphate buffer supplemented with 0.1% (v/v) Triton-X100 and benzonase (25mM Kpi pH6.5, 0.1% Triton-X100 and 25U/mL benzonase) and lysed using sonication (20% amplitute, 3s on, 3s off for 4 cycles) while on ice. Protein concentration was determined (BCA kit; Pierce, Thermo Fisher) with BSA as standard.

Enzyme activity assay
General activity procedures – Generally ,assays were performed using homogenate in KPi lysis buffer (12.5 µL, ± 12.5 µg protein) by addition of McIlvaine buffer (citric acid – Na_2HPO_4) of the appropriate pH (12.5 µL; 150mM McIlvaine pH4 or pH5.2) before addition of 4-methylumbelifferyl β-glucoside mix. Assays were performed using 4MU-β-Glc mixes optimized for each protein; 100 µL of 3.75 mM 4MU-β-Glc substrate, 0.1% (w/v) BSA, 0.1% (v/v) Triton-X and 0.2% (w/v) Sodium Taurocholate at pH5.2 for human GCase (pH5.2++), 3.75 mM 4MU-β-Glc substrate and 0.1% (w/v) BSA at pH 4 for zebrafish and frog GCase (pH4--) and 3.75 mM 4MU-β-Glc substrate and 0.1% (w/v) BSA at pH 5.2 for turtle GCase (pH 5.2--). Incubation was performed for 30min at 37 °C and stopped by addition of glycine-NaOH STOP buffer (200 µL; 1 M Glycine-NaOH, pH 10.3) unless stated otherwise. All activity assays were measured using a LS-55 (PerkinElmer, Waltham, USA; λ_{ex} of 366 nm, λ_{em} of 445nm) and calculated using a standard of 1nmol 4MU. All activities were measured using three independent homogenates measured in technical duplicate unless indicated otherwise in the result section.
pH curves – PH curves were obtained by incubating homogenate (12.5 µL, ± 12.5 µg total protein) with McIlvaine of the appropriate pH (62.5 µL; 300 mM McIlvaine, pH 2-8) on ice for 5 minutes before addition of two-times concentrated Glc-4Mu substrate mix with additives (50 µL; 7,5 mM Glc-4Mu, 0.2% (w/v) BSA, 0.2% (v/v) Triton-X and 0.4% (w/v) Sodium Taurocholate in MilliQ) or without additives (50 µL; 7.5 mM GlcMu and 0.2% (w/v) BSA in MilliQ).
Michaelis-Menten kinetics – To homogenate (12.5 µL, ± 12.5 µg protein) was added McIlvaine with the appropriate pH (12.5 µL, 150 mM McIlvaine pH 4 or pH 5.2) and subsequently incubated with different substrate concentrations (100 µL; 0-10 mM Glc-4Mu +0.1% (w/v) BSA in either 150 mM McIlvaine buffer pH 4 (pH4--), 150 mM McIlvaine buffer pH 5.2 or 150 mM McIlvaine buffer pH 5.2 + 0.1% (v/v) Triton-X + 0.2% (w/v) Sodium Taurocholate (pH5.2++)). K_m and V_{max} values were calculated using Graphpad Prism 8.0 (GraphPad Software, San Diego, USA).
Temperature curve – Homogenates were incubated with 4MU-β-Glc mixes in PCR tubes as described in the general assay procedures and incubated at different temperatures. At indicated time points, 5 µL of the sample was removed from the mixture, added to 200 µL STOP buffer and the fluorescence was measured and calculated in pmol/h/mg. The relative activity was calculated using the activity of the respective GCase at 30 min and 37 °C incubation.
IC_{50} curve – For the covalent GCase specific inhibitor, human or zebrafish GCase expressing cell homogenate (12.5 µL, ± 12.5 µg protein) was pre-incubated with ME656 (2x concentrated in 300 mM McIlvaine pH 4 or pH 5.2 with 1% (v/v) DMSO) for 30 min at 37 ° before addition of the respective 4MU-β-Glc mix, incubation and measurement in the general assay procedures. IC_{50} curves were fitted using GraphPad Prism.
Saposin C/phosphatidylserine activation - Phosphatidylserine (PS, 10 mg/mL in chloroform/ methanol) was concentrated and resuspended in McIlvaine buffer (2x concentrated 'PS mix'; 80 µg/mL PS, 300 mM McIlvaine pH 4 or pH 5.2). Recombinant human Saposin C (900 µg/µL) was diluted in McIlvaine buffer (50 µg/µL, 300 mM McIlvaine buffer pH 4 or pH 5.2). To human or zebrafish GCase expressing cell homogenates (12.5 µL, 12.5 µg protein) was added Saposin C mix or McIlvaine (12.5µL), 'PS mix' or McIlvaine (50 µL) and 4MU-β-Glc mix (2x concentrated, 50 µL; 7.5 mM 4MU-β-Glc and 0.2% (w/v) BSA in MilliQ or 50 µL of 7.5 mM 4MU-β-Glc, 0.2% (w/v) BSA, 0.2% (v/v) Triton-X and 0.4% (w/v) Sodium Taurocholate in MilliQ). Assays were incubated and measured as described above.

Activity-based probe (ABP) labelling

General ABP labelling procedures – Homogenates (10 µL, 10 µg total protein or protein amount to obtain equal activity towards 4MU-β-Glc) was labelled with the cy5-modified cyclophellitol-epoxide ABP ME569 (200 nM ME569 in 10 µl 300 mM McIlvaine buffer pH 4 or 5.2, without additives or supplemented with 0.2% (v/v) Triton-X100 and 0.4% (w/v) Sodium Taurocholate for human GCase, 1% (v/v) DMSO; final concentration 100 nM ME569 and 0.5% (v/v) DMSO). Proteins were denatured with 5x Laemmli sample buffer (25% (v/v) 1.25 M Tris-HCL pH 6.8, 50% (v/v) 100% glycerol, 10% (w/v) sodium dodecyl sulfate (SDS), 8% (w/v) dithiothreitol (DTT) and 0.1% (w/v) bromophenol blue) and boiled for 5 min at 98 °C. ABP-labelled protein samples were separated by electrophoreses on 10% (w/v) SDS-PAGE gels, before scanning the fluorescence of the wet-slab gel with a Typhoon FLA 9500 (GE Healthcare, Chicaco, USA; cy5 (λ_{ex} of 635 nm, λ_{em} of 655-685 nm), 750 V, pixel size 100 µM). Gels wer stained with Coomassie Brilliant Blue staining or transferred to a nitrocellulose membrane (BioRad, Hercules, USA).

Deglycosylation using PNGase F – Glycoproteins were deglycosylated using PNFase F (NEB, Ipswich, USA). Briefly, homogenate was labelled with ME569, as described above, in 2x volumes (40 µL final volume). After incubation for 30 min at 37 °C, the mixture was denatured using Glycoprotein buffer (supplied) and boiled for 10 min at 98 °C. The sample was divided, NP-40 (supplied) and MQ was added to both samples NP-40 and one 20 µL sample was incubated with PNGase F, while the other 20 µL sample was incubated with MQ for 1 h at 37 °C. Laemmli sample buffer (5x) was added after incubation and the samples were separated on a 10% (w/v) SDS-PAGE gel and scanned as described.

Immunoblot – Proteins were transferred to a 0.2 µm nitrocellulose membrane by Trans-Blot Turbo™ transfer system (Bio-Rad). Membrane was blocked with 5% (w/v) BSA in TBST for 1 h at rt and incubated overnight at 4 °C with primary antibody (anti-GCase, Sigma-Aldrich G4171; 1:1000). Membrane was washed three times with TBST and incubated with secondary antibody (goat anti-rabbit IgG (H+L)-HRP, Bio-Rad; 1:5000) for 1 h at 37 °C, washed twice with TBST and a final time with TBS before development using the Clarity Max ECL substrates (Bio-Rad) and detected by the ChemiDoc™ MP system (Bio-Rad).

Transglucosylation and GlcChol hydrolysis

General transglucosylation using LC-MS/MS measurement – Generally, transglucosylation activity of was determined with 4MU-β-Glc as donor and natural cholesterol as acceptor, as described with minor modifications [18]. Briefly, to GCase expressing cell homogenates (12.5 µL, ± 40-50 µg total protein) was added a mix of cholesterol acceptor and 4MU-β-Glc donor in McIlvaine buffer of the appropriate pH and supplemented with additives (100 µL including 3.75 mM 4MU-β-Glc, 0.1% (w/v) BSA and 25 µM cholesterol with 1% ethanol in 150 mM McIlvaine pH 4 or pH 5.2 supplemented with 0.1% (v/v) Triton-X100 and/or 0.2% (w/v) Sodium Taurocholate). After 1 h incubation at 37 °C with shaking, 5 µL of the sample was transferred in duplicate to 200 µL STOP buffer, 4MU was measured and enzymatic activity was calculated. The residual sample was snap-frozen in liquid nitrogen or $^{13}C_6$-GlcChol internal standard (20 µL, 0.1 pmol/µL in methanol) was added to the 115 µL of remaining sample, followed by methanol and chloroform (2:1 (v/v)) to precipitate the protein. After centrifugation, lipids of the supernatant were extracted using a Bligh-Dyer extraction (MeOH:$CHCl_3$:H_2O, 1:1:0.9) and measured using previously described methods[18].

GlcChol hydrolysis – An appropriate volume of GlcChol (2 pmol per reaction) was concentrated and resuspended in ethanol to a concentration of 1.6 pmol/µL. A mixture of GlcChol in McIlvaine of the appropriate pH was prepared with BSA (0.1 % (w/v)) and with the necessary additives for every GCase enzymes as described in the result section (0.1% (v/v) Triton-X100) and/ or 0.2% (w/v) Sodium Taurocholate). GCase expressing cell homogenates (12.5 µL, ± 40-50 µg total protein) were incubated with vehicle or the GCase specific inhibitor ME656 (12.5 µL of 2µM ME656 in 300 mM McIlvaine pH 4 or pH 5.2, 1% (v/v) DMSO) for 30 min at 37 °C before addition of the GlcChol mix (100 µL; 1.25 µL GlcChol (1.6 pmol/µL in ethanol) in 150 mM McIlvaine pH 4 or pH 5.2, 0.1% (w/v) BSA, 0.1% (v/v) Triton-X100 and/or 0.2% (w/v) Sodium Taurocholate; final ethanol concentration of 1% (v/v)).

Samples were incubated for 1 h or overnight (17 hours) at 37 °C, stopped by addition of internal standard, methanol and chloroform and subsequently extracted using the Bligh-Dyer extraction and lipid measurements as described for the transglucosylation.

Transglucosylation with NBD-lipids and HPTLC – NBD modified lipids including N-[12-[(7-nitro-2-1,3-benzoxadiazol-4-yl)amino]dodecanoyl]-d-erythro-sphingosine (C12-NBD-Cer), N-[6-[(7-Nitro-2-1,3-benzoxadiazol-4-yl)amino]caproyl]-D-glucosyl-β1-1'-sphingosine (C6-NBD-Spho) and 25-[N-[(7-nitro-2-1,3-benzoxadiazol-4-yl)methyl]amino]-27-norcholesterol (NBD-Chol) were purchased from Sigma or Avanti Polar lipids (Alabaster, USA). To GCase expressing cell homogenates (12.5 µL, ± 40-50 µg total protein) was added McIlvaine with the appropriate pH (12.5 µL 150 mM McIlvaine pH 4 or pH 5.2) and a mixture of 4MU-β-Glc as glucose donor and NBD-lipid as acceptor in McIlvaine buffer pH 4 or pH 5.2 with or without appropriate additives (100 µL; 1.25 µL NBD-lipid (in 100% ethanol; 1% final concentration) in 150 mM McIlvaine pH 4 or pH 5.2, 0.1% (w/v) BSA without additives or supplemented with 0.1% (v/v) Triton-X100 and/ or 0.2% (w/v) Sodium Taurocholate. Final concentration of the NBD-lipids: 20 µM for NBD-Chol, 10 µM for NBD-Cer and 10 µM for NBD-Sph. Samples were incubated for 1 h at 37 °C and lipids were extracted using the Bligh- Dyer extraction as described above. Lipids were reconstituted in 20 µL methanol and separated by thin layer chromatography on HPTLC silica gel 60 plates using $CHCl_3$:MeOH (80:20, v/v) as eluent. The HPTLC plate with NBD-lipids was scanned using a Typhoon imaging system (cy2 settings (λ_{ex} of 488 nm, λ_{em} of 515-535 nm), 250 V, pixel size 100 µM

Alignment and modelling – For alignment and modelling sequences of zebrafish (Uniprot code E7EZM1), frog (Uniprot code A0A1L8FDF0) and turtle (NCBI code XP_005280735) GCase were used. Signal peptides were predicted using SignalP5.0[43] and sequences without predicted signal peptides were aligned with Clustal Omega[44]. Zebrafish, frog and turtle structures were modelled with Swiss-Model[45] using the established 3D-structure of human GCase associated with 5N,6S-(N'-(N-octyl)imino)-6-thionojirimycin (6S-NOI-NJ) in the catalytic pocket (PDB 2XWE[36]) as search model. Structures were superimposed and visualized with CCP4MG[46] with glucose docked at the 6S-NOI-NJ ligand position. For alignment of predicted GCase sequences of additional species were used: python (*Python bivittatus*, NCBI code XP_007435239), goose (*Anser cygnoides domesticus*, NCBI code XP_013055943), saltwater crocodile (*Crocodylus porosus*, NCBI code XP_019412408), freshwater crocodile (*Gavialis gangetus*, NCBI code XP_019383528), dolphin (*tursiops truncates*, NCBI code XP_004315654) and mouse (*Mus musculus*, NCBI code NP_032120)

References

1. Brady R.O., Kanfer J.N., Bradley R.M.and Shapiro D. (1966) Demonstration of a deficiency of glucocerebroside-cleaving enzyme in Gaucher's disease. *The Journal of clinical investigation* **45**, 1112-1115.
2. Van Weely S., Aerts J.M., Van Leeuwen M.B., Heikoop J.C., Donker-Koopman W.E., Barranger J.A.,... and Schram A.W. (1990) Function of oligosaccharide modification in glucocerebrosidase, a membrane-associated lysosomal hydrolase. *Eur J Biochem* **191**, 669-677.
3. Berg-Fussman A., Grace M.E., Ioannou Y.and Grabowski G.A. (1993) Human acid beta-glucosidase. N-glycosylation site occupancy and the effect of glycosylation on enzymatic activity. *J Biol Chem* **268**, 14861-14866.
4. Reczek D., Schwake M., Schroder J., Hughes H., Blanz J., Jin X.,... and Saftig P. (2007) LIMP-2 is a receptor for lysosomal mannose-6-phosphate-independent targeting of beta-glucocerebrosidase. *Cell* **131**, 770-783.
5. Zunke F., Andresen L., Wesseler S., Groth J., Arnold P., Rothaug M.,... and Schwake M. (2016) Characterization of the complex formed by beta-glucocerebrosidase and the lysosomal integral membrane protein type-2. *Proc Natl Acad Sci U S A* **113**, 3791-3796.
6. Rijnboutt S., Aerts H.M., Geuze H.J., Tager J.M.and Strous G.J. (1991) Mannose 6-phosphate-independent membrane association of cathepsin D, glucocerebrosidase, and sphingolipid-activating protein in HepG2 cells. *J Biol Chem* **266**, 4862-4868.
7. Saftig P.and Klumperman J. (2009) Lysosome biogenesis and lysosomal membrane proteins: trafficking meets function. *Nat Rev Mol Cell Biol* **10**, 623-635.
8. Aerts J.M., Schram A.W., Strijland A., van Weely S., Jonsson L.M., Tager J.M.,... and Murray G.J. (1988) Glucocerebrosidase, a lysosomal enzyme that does not undergo oligosaccharide phosphorylation. *Biochimica et biophysica acta* **964**, 303-308.
9. Tylki-Szymanska A., Czartoryska B., Vanier M.T., Poorthuis B.J., Groener J.A., Lugowska A.,... and Jurkiewicz E. (2007) Non-neuronopathic Gaucher disease due to saposin C deficiency. *Clin Genet* **72**, 538-542.
10. Tylki-Szymanska A., Groener J.E., Kaminski M.L., Lugowska A., Jurkiewicz E.and Czartoryska B. (2011) Gaucher disease due to saposin C deficiency, previously described as non-neuronopathic form--no positive effects after 2-years of miglustat therapy. *Mol Genet Metab* **104**, 627-630.
11. Vaccaro A.M., Motta M., Tatti M., Scarpa S., Masuelli L., Bhat M.,... and Salvioli R. (2010) Saposin C mutations in Gaucher disease patients resulting in lysosomal lipid accumulation, saposin C deficiency, but normal prosaposin processing and sorting. *Human molecular genetics* **19**, 2987-2997.
12. Dvir H., Harel M., McCarthy A.A., Toker L., Silman I., Futerman A.H.and Sussman J.L. (2003) X-ray structure of human acid-beta-glucosidase, the defective enzyme in Gaucher disease. *EMBO Rep* **4**, 704-709.
13. Smith L., Mullin S.and Schapira A.H.V. (2017) Insights into the structural biology of Gaucher disease. *Exp Neurol* **298**, 180-190.
14. Ben Bdira F., Artola M., Overkleeft H.S., Ubbink M.and Aerts J. (2018) Distinguishing the differences in beta-glycosylceramidase folds, dynamics, and actions informs therapeutic uses. *J Lipid Res* **59**, 2262-2276.
15. Rye C.S.and Withers S.G. (2000) Glycosidase mechanisms. *Current opinion in chemical biology* **4**, 573-580.
16. Witte M.D., Kallemeijn W.W., Aten J., Li K.Y., Strijland A., Donker-Koopman W.E.,... and Aerts J.M. (2010) Ultrasensitive in situ visualization of active glucocerebrosidase molecules. *Nature chemical biology* **6**, 907-913.
17. Kallemeijn W.W., Li K.Y., Witte M.D., Marques A.R., Aten J., Scheij S.,... and Overkleeft H.S. (2012) Novel activity-based probes for broad-spectrum profiling of retaining beta-exoglucosidases in situ and in vivo. *Angewandte Chemie* **51**, 12529-12533.
18. Marques A.R., Mirzaian M., Akiyama H., Wisse P., Ferraz M.J., Gaspar P.,... and Aerts J.M. (2016) Glucosylated cholesterol in mammalian cells and tissues: formation and degradation by multiple cellular beta-glucosidases. *J Lipid Res* **57**, 451-463.
19. Akiyama H.and Hirabayashi Y. (2017) A novel function for glucocerebrosidase as a regulator of sterylglucoside metabolism. *Biochim Biophys Acta Gen Subj* **1861**, 2507-2514.
20. Akiyama H., Nakajima K., Itoh Y., Sayano T., Ohashi Y., Yamaguchi Y.,... and Hirabayashi Y. (2016) Aglycon diversity of brain sterylglucosides: structure determination of cholesteryl- and sitosterylglucoside. *J Lipid Res* **57**, 2061-2072.
21. Brumshtein B., Greenblatt H.M., Butters T.D., Shaaltiel Y., Aviezer D., Silman I.,... and Sussman J.L. (2007) Crystal structures of complexes of N-butyl- and N-nonyl-deoxynojirimycin bound to acid beta-glucosidase: insights into the mechanism of chemical chaperone action in Gaucher disease. *J Biol Chem* **282**, 29052-29058.
22. Lieberman R.L., D'Aquino J A., Ringe D.and Petsko G.A. (2009) Effects of pH and iminosugar pharmacological chaperones on lysosomal glycosidase structure and stability. *Biochemistry* **48**, 4816-4827.
23. Lieberman R.L. (2011) A Guided Tour of the Structural Biology of Gaucher Disease: Acid-beta-Glucosidase and Saposin C. *Enzyme Res* **2011**, 973231.

24. Kacher Y., Brumshtein B., Boldin-Adamsky S., Toker L., Shainskaya A., Silman I.,... and Futerman A.H. (2008) Acid beta-glucosidase: insights from structural analysis and relevance to Gaucher disease therapy. *Biol Chem* **389**, 1361-1369.
25. van Smeden J., Dijkhoff I.M., Helder R.W.J., Al-Khakany H., Boer D.E.C., Schreuder A.,... and Bouwstra J.A. (2017) In situ visualization of glucocerebrosidase in human skin tissue: zymography versus activity-based probe labeling. *J Lipid Res* **58**, 2299-2309.
26. Chan A., Holleran W.M., Ferguson T., Crumrine D., Goker-Alpan O., Schiffmann R.,... and Sidransky E. (2011) Skin ultrastructural findings in type 2 Gaucher disease: diagnostic implications. *Mol Genet Metab* **104**, 631-636.
27. Doering T., Holleran W.M., Potratz A., Vielhaber G., Elias P.M., Suzuki K.and Sandhoff K. (1999) Sphingolipid activator proteins are required for epidermal permeability barrier formation. *J Biol Chem* **274**, 11038-11045.
28. Holleran W.M., Ginns E.I., Menon G.K., Grundmann J.U., Fartasch M., McKinney C.E.,... and Sidransky E. (1994) Consequences of beta-glucocerebrosidase deficiency in epidermis. Ultrastructure and permeability barrier alterations in Gaucher disease. *The Journal of clinical investigation* **93**, 1756-1764.
29. Keatinge M., Bui H., Menke A., Chen Y.C., Sokol A.M., Bai Q.,... and Bandmann O. (2015) Glucocerebrosidase 1 deficient Danio rerio mirror key pathological aspects of human Gaucher disease and provide evidence of early microglial activation preceding alpha-synuclein-independent neuronal cell death. *Human molecular genetics* **24**, 6640-6652.
30. Zancan I., Bellesso S., Costa R., Salvalaio M., Stroppiano M., Hammond C.,... and Moro E. (2015) Glucocerebrosidase deficiency in zebrafish affects primary bone ossification through increased oxidative stress and reduced Wnt/beta-catenin signaling. *Human molecular genetics* **24**, 1280-1294.
31. Aerts J.M., Sa Miranda M.C., Brouwer-Kelder E.M., Van Weely S., Barranger J.A.and Tager J.M. (1990) Conditions affecting the activity of glucocerebrosidase purified from spleens of control subjects and patients with type 1 Gaucher disease. *Biochimica et biophysica acta* **1041**, 55-63.
32. Artola M., Kuo C.L., Lelieveld L.T., Rowland R.J., van der Marel G.A., Codee J.D.C.,... and Overkleeft H.S. (2019) Functionalized Cyclophellitols Are Selective Glucocerebrosidase Inhibitors and Induce a Bona Fide Neuropathic Gaucher Model in Zebrafish. *Journal of the American Chemical Society* **141**, 4214-4218.
33. Hruska K.S., LaMarca M.E., Scott C.R.and Sidransky E. (2008) Gaucher disease: mutation and polymorphism spectrum in the glucocerebrosidase gene (GBA). *Hum Mutat* **29**, 567-583.
34. Lieberman R.L., Wustman B.A., Huertas P., Powe A.C., Jr., Pine C.W., Khanna R.,... and Petsko G.A. (2007) Structure of acid beta-glucosidase with pharmacological chaperone provides insight into Gaucher disease. *Nature chemical biology* **3**, 101-107.
35. Martinez-Bailen M., Carmona A.T., Patterson-Orazem A.C., Lieberman R.L., Ide D., Kubo M.,... and Moreno-Vargas A.J. (2019) Exploring substituent diversity on pyrrolidine-aryltriazole iminosugars: Structural basis of beta-glucocerebrosidase inhibition. *Bioorg Chem* **86**, 652-664.
36. Brumshtein B., Aguilar-Moncayo M., Benito J.M., Garcia Fernandez J.M., Silman I., Shaaltiel Y.,... and Ortiz Mellet C. (2011) Cyclodextrin-mediated crystallization of acid beta-glucosidase in complex with amphiphilic bicyclic nojirimycin analogues. *Organic & biomolecular chemistry* **9**, 4160-4167.
37. Sultana S., Truong N.Y., Vieira D.B., Wigger J.G., Forrester A.M., Veinotte C.J.,... and van der Spoel A.C. (2016) Characterization of the Zebrafish Homolog of beta-Glucosidase 2: A Target of the Drug Miglustat. *Zebrafish* **13**, 177-187.
38. Kuo C.L., Kallemeijn W.W., Lelieveld L.T., Mirzaian M., Zoutendijk I., Vardi A.,... and Artola M. (2019) In vivo inactivation of glycosidases by conduritol B epoxide and cyclophellitol as revealed by activity-based protein profiling. *FEBS J* **286**, 584-600.
39. Lelieveld L.T., Mirzaian M., Kuo C.L., Artola M., Ferraz M.J., Peter R.E.A.,... and Aerts J. (2019) Role of beta-glucosidase 2 in aberrant glycosphingolipid metabolism: model of glucocerebrosidase deficiency in zebrafish. *J Lipid Res* **60**, 1851-1867.
40. Aerts J., Kuo C.L., Lelieveld L.T., Boer D.E.C., van der Lienden M.J.C., Overkleeft H.S.and Artola M. (2019) Glycosphingolipids and lysosomal storage disorders as illustrated by gaucher disease. *Current opinion in chemical biology* **53**, 204-215.
41. Do H.V. (2017) Variant, recombinant beta-glucocerebrosidase proteins with increased stability and increased retained catalytic activity **Volume US9254313B2**. (United States: Amicus Therapeutics Inc).
42. Ben Bdira F., Kallemeijn W.W., Oussoren S.V., Scheij S., Bleijlevens B., Florea B.I.,... and Aerts J. (2017) Stabilization of Glucocerebrosidase by Active Site Occupancy. *ACS Chem Biol* **12**, 1830-1841.
43. Almagro Armenteros J.J., Tsirigos K.D., Sonderby C.K., Petersen T.N., Winther O., Brunak S.,... and Nielsen H. (2019) SignalP 5.0 improves signal peptide predictions using deep neural networks. *Nat Biotechnol* **37**, 420-423.
44. Madeira F., Park Y.M., Lee J., Buso N., Gur T., Madhusoodanan N.,... and Lopez R. (2019) The EMBL-EBI search and sequence analysis tools APIs in 2019. *Nucleic acids research* **47**, W636-W641.

45. Waterhouse A., Bertoni M., Bienert S., Studer G., Tauriello G., Gumienny R.,... and Schwede T. (2018) SWISS-MODEL: homology modelling of protein structures and complexes. *Nucleic acids research* **46**, W296-W303.
46. McNicholas S., Potterton E., Wilson K.S.and Noble M.E. (2011) Presenting your structures: the CCP4mg molecular-graphics software. *Acta Crystallogr D Biol Crystallogr* **67**, 386-394.